Materials Today Bio 29 (2024) 101310

Contents lists available at ScienceDirect

Materials Today Bio

journal homepage: www.journals.elsevier.com/materials-today-bio

Procyanidin capsules provide a new option for long-term ROS scavenging in chronic inflammatory diseases

Linxiao Sun [a,b,1], Shaoyin Wei [c,1], Chenglong Wang [d], Yipiao Zhang [e,f], Xingjie Zan [c,*], Lianxin Li [d,**], Chunwu Zhang [b,***]

[a] Department of Laboratory, Guizhou Provincial People's Hospital, Guiyang, Guizhou, 550002, China
[b] The First Affiliated Hospital of Wenzhou Medical University, Wenzhou, 325000, Zhejiang, China
[c] Wenzhou Institute, University of Chinese Academy of Sciences, Wenzhou, 325001, Zhejiang, China
[d] Department of Orthopaedics Surgery, Shandong Provincial Hospital Affiliated to Shandong First Medical University, Jinan, 250021, Shandong, China
[e] Collaborative Innovation Center of Yangtze River Delta Region Green Pharmaceuticals, No. 18, Chaowang Road, Gongshu District, Zhejiang University of Technology, Hangzhou, Zhejiang 310014, China
[f] Zhejiang Provincial Key Laboratory of TCM for Innovative R&D and Digital Intelligent Manufacturing of TCM Great Health Products, Huzhou, 313200, China

ARTICLE INFO

Keywords:
Procyanidin capsules
Long-term ROS scavenging
Diabetic wounds
Osteoarthritis

ABSTRACT

Chronic inflammatory diseases such as diabetic wounds and osteoarthritis are significant threats to human health. Failure to scavenge longstanding excessive reactive oxygen species (ROS) is an important cause of chronic inflammatory diseases, yet existing treatments that provide long-lasting therapeutic effects are limited. Here, procyanidin capsules were synthesized in a simple one-step way using calcium carbonate as a template. The biosafety of procyanidin capsules *in vitro* and *in vivo* was monitored by cytotoxicity and pathological sections. The therapeutic effect of procyanidin capsules in diabetic wounds and osteoarthritis was accessed by pathological evaluation combined with the quantification of inflammatory markers. The data showed that procyanidin capsules could long-term scavenge excessive ROS and effectively promote articular cartilage repair in osteoarthritis, accelerating diabetic wound healing. Lastly, transcriptome analysis suggested that procyanidin capsules commonly regulated adenosine 5′-monophosphate (AMP)-activated protein kinase (AMPK) signaling in diabetic wounds and osteoarthritis. This study provides a straightforward protocol for creating procyanidin capsules, while presenting a promising new therapeutic option for long-term scavenging ROS in chronic inflammatory diseases.

1. Introduction

At the sites of chronic inflammatory disease lesions persist excessively produced reactive oxygen species (ROS) including hydrogen peroxide (H_2O_2), singlet oxygen ($^1O_2$), superoxide anion ($O_2^{\bullet-}$), and hydroxyl radical ($^{\bullet}OH$) [1–3]. Uninterrupted overproduced ROS trigger tissue continuous inflammatory reaction and injury. The longstanding redundant ROS not adequately and timely cleared by the ROS scavenging system act as critical mediators of chronic inflammatory diseases such as diabetic wounds and osteoarthritis [4,5]. Diabetic wounds are prevalent among patients with diabetes and constitute a significant challenge due to their chronicity and tendency to become complex and recalcitrant, it can result in skin itching and may lead to tissue ulceration and even amputation [6]. Osteoarthritis as another prevalent chronic disease affecting over 500 million individuals globally will not only cause swelling and pain of joints but also lead to joint deformity and limb paralysis in serious cases [7]. However, the course of diabetic wounds and osteoarthritis as well as many other chronic inflammatory diseases often extends over several months or even years, and existing treatments fail to consistently remove long-term excessive ROS from the site of inflammatory lesions [8,9].

Based on the main functions of ROS in cells, organelles, and related

* Corresponding author.
** Corresponding author.
*** Corresponding author.
E-mail addresses: zanxj@ucas.ac.cn (X. Zan), 13505312449@163.com (L. Li), zcw6681@wmu.edu.cn (C. Zhang).
[1] Equal contribution authors.

https://doi.org/10.1016/j.mtbio.2024.101310
Received 21 August 2024; Received in revised form 13 October 2024; Accepted 24 October 2024
Available online 24 October 2024

clearance enzymes, corresponding categories of biomaterials have been developed to scavenge ROS [10–12]. Wen et al. developed lanthanide nanoparticles equipped with a peptide coating that effectively prevented the additionally generated production of ROS in macrophages [13]. Ouyang et al. employed the sulfur trioxide-pyridine technique to produce polysaccharides-based biomaterials that effectively attenuated the decrease in mitochondrial membrane potential, ultimately leading to a reduction in ROS levels associated with kidney stone-induced inflammation [14]. Shi et al. have devised a strategy to develop a few-layered niobium carbide (Nb2C) nanostructure that could effectively adsorb excessive ROS to improve osteolytic inflammatory response [15]. The above-mentioned biomaterials provide valuable references for ROS clearance research, but most of these systems can only achieve immediate and short-term ROS clearance, and cannot have long-term and sustained effects, which limits their application in chronic diseases.

Numerous studies have shown that consuming fruits and vegetables regularly can lead to better health and lower risk of chronic diseases [16,17]. One of the reasons is natural polyphenols from fruits and vegetables that can timely eliminate excessive ROS [18–20]. Maintaining the habit of consuming fruits and vegetables for a long time can reduce many ROS-related chronic inflammatory diseases [21,22]. The development of polyphenolic biomaterials that simulate daily intake of fruits and vegetables has drawn significant attention among researchers due to the potential to deliver polyphenols in a sustained manner. Some polyphenol-based biomaterials exhibit good long-term ROS scavenging ability. Liu et al. conjugated tannic acid with phenylboronic acid-modified polyphosphazene and poly (vinyl alcohol) to develop a nanoparticle hydrogel that effectively removed excessive ROS from diabetic wounds for up to 14 days compared to the Tegaderm control group [23]. Chen et al. designed and developed a novel double-layered poly (lactic-co-glycolic acid) (PLGA)/sodium hyaluronate (HA) microneedle system as a long-acting formulation of polyphenols for the effective and sustained management of atopic dermatitis [24]. Although these polyphenolic biomaterials prolonged ROS scavenging clearance time, the preparation of these polyphenols is somewhat complex and incorporates non-natural compounds such as nitriles, which impedes their potential clinical applications. The current research objectives aim to simplify the synthesis process and minimize the presence of non-polyphenolic compounds in the synthetic materials, thereby enhancing biocompatibility and increasing the likelihood of long-term reduction in ROS and mitigating chronic inflammation.

Herein, we design a novel type of procyanidin capsules with good biocompatibility and excellent long-term ROS scavenging ability. Based on the template removing measure, the procyanidin (PC) was mixed with calcium carbonate ($CaCO_3$), then the $CaCO_3$ template was removed rapidly by hydrogen chloride (HCl), and procyanidin capsules were prepared (Fig. 1A). The method is particularly simple and the whole reaction process only takes one step. The stability and long-lasting ROS scavenging ability of procyanidin capsules, as well as the therapeutic effects and potential molecular targeted signaling of procyanidin capsules on diabetic wounds and osteoarthritis have been evaluated in detail (Fig. 1B and C). Our results demonstrated that procyanidin capsules were stable under multiple conditions and could effectively clear ROS for a long time to combat chronic inflammatory diseases.

2. Materials and methods

2.1. Materials

Sodium carbonate anhydrous (Na_2CO_3), calcium chloride anhydrous

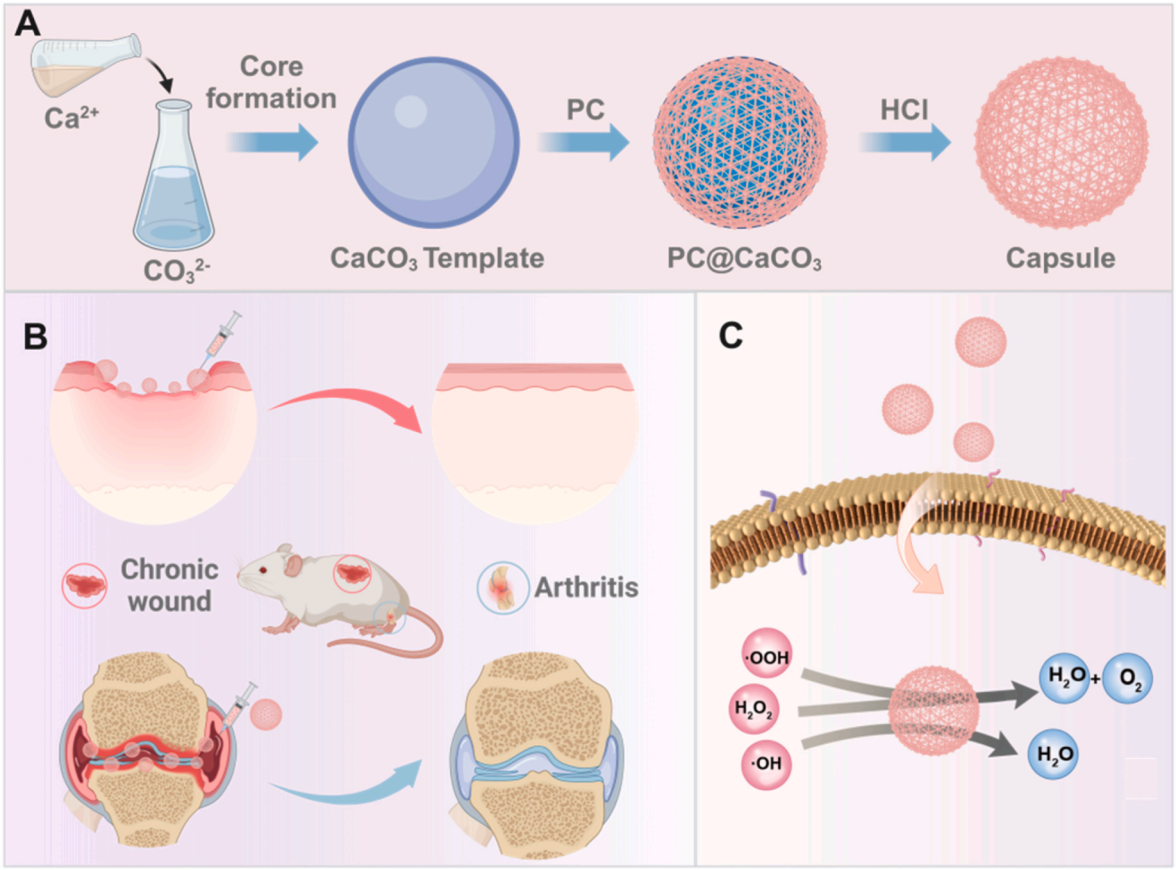

Fig. 1. Procyanidin capsules combats chronic inflammation via ROS scavenging. (A) Schematic diagram of the preparation routes of procyanidin capsules. (B) Schematic of procyanidin capsules treatment in streptozotocin (STZ) induced diabetic wounds or surgically constructed osteoarthritis model. (C) procyanidin capsules could long-term scavenge ROS including •OH, •OOH, and H_2O_2.

($CaCl_2$), procyanidin (PC), hydrogen peroxide (H_2O_2), hydrochloric acid (HCl), xylenol orange, and sodium hydroxide (NaOH) were purchased from Aladdin Industrial (Shanghai, China). The total antioxidant capacity assay and superoxide assay kits were purchased from Beyotime Biotechnology (Shanghai, China). The 2,2-diphenyl-1-picrylhydrazyl (DPPH) radical scavenging capacity assay kit, 2,2′-azino-bis(3-ethylbenzothiazoline-6-sulfonate) ABTS radical scavenging capacity assay kit, 4′,6-diamidino-2-phenylindole dihydrochloride (DAPI), TRITC-phalloidin and 2,7-dichlorodihydrofluorescein diacetate (DCF-DA), radioimmunoprecipitation assay (RIPA) lysate (R0010), PMSF (P0100), BCA protein concentration determination kit (PC0020) were obtained from Solarbio Science (Shanghai, China). Cell Counting Kit-8 (CCK-8) was purchased from Dojindo Molecular Technologies (Shanghai, China). Anti-mouse ELISA kits for IL-6 and TNF-α were obtained from Thermo Fisher Scientific (Beijing, China). All reagents and materials were used without further purification. RAW 264.7 and DC2.4 cells were obtained from the Culture Collection of the Chinese Academy of Sciences (Shanghai, China). Antibodies: anti-Pck1 (K007662P), anti-Prkaa2 (K106707P), and anti-GAPDH (K000026M) were from solaria (Beijing, China). Male 6-week-old C57BL/6 mice were purchased from Shanghai SLAC Laboratory Animal (SLAC). All animal experiments were approved by the Wenzhou Medical University Institutional Animal Care and Use Committee.

2.2. Synthesis of procyanidin capsules

Pure calcium carbonate ($CaCO_3$) was synthesized as described [25]. Briefly, 0.33 M Na_2CO_3 and 0.33 M $CaCl_2$ were mixed in equal volumes in a conical flask. After stirring for 40 s at 1200 rpm, the formed particles were collected through centrifugation at a speed of 1000 rpm for 3 min, and subsequently subjected to three thorough washes with deionized water. The pure $CaCO_3$ was freeze dried. To prepare the procyanidin capsules, procyanidin was dissolved in deionized water and adjusted to pH 8.0 with 2 M NaOH, the concentration of procyanidin solution was 60 mg/mL. Pure $CaCO_3$ microparticles (~10 mg) were dispersed in 3 mL above the procyanidin solution. After shaking for 12 h, 24 h, 48 h, and 72 h, the PC coated $CaCO_3$ (PC@$CaCO_3$) microparticles were collected by centrifugation (1000 rpm, 5 min), then washed three times with deionized water. The capsules were obtained by incubating the PC@$CaCO_3$ microparticles in 1 M HCl solution for 10 s to remove the $CaCO_3$ core completely. The spherical capsules were collected by centrifugation (3000 rpm, 5 min) and washed at least five times with deionized water. The procyanidin capsules were used in all the following experiments. Procyanidin capsules made from polystyrene microspheres or silica sphere templates were prepared by the same method, except that the $CaCO_3$ templates were replaced, and the incubation period was 72 h. Tetrahydrofuran was used to remove the templates, and hydrofluoric acid was used to remove the silica templates.

2.3. Characterization of procyanidin capsules

UV–vis spectra were obtained by an ultraviolet–visible-near red spectrophotometry (CARY 5000, USA). Sample absorbance was detected on a Lambda 25 spectrophotometer (PerkinElmer, USA). The surface morphology and dispersibility of the spherical capsules were characterized by scanning electron microscopy (SEM, FESEM, SU8010 HITACHI), transmission electron microscopy (TEM, FEI Talos F200S microscope), optical microscopy (OM, NIKON Ni-U), and confocal laser confocal microscopy (CLSM, Nikon A1). The formation of capsules was characterized by Fourier transforms infrared (FTIR) spectroscopy (Bruker TENSOR II) and X-ray photoelectron spectroscopy (Thermo-Electron ESCALAB 250). Scavenging of ROS and active nitrogen and superoxide radical was detected by total antioxidant capacity, ferrous oxidation-xylenol (FOX), superoxide scavenging capacity, DPPH free radical scavenging, ABTS free radical scavenging assay kits, and superoxide scavenging capacity assay kits. All scavenging assays were carried out with kits according to the manufacturer instructions.

2.4. In vitro and in vivo biocompatibility

Cytotoxicity was measured in RAW 264.7 and DC2.4 cells using a CCK-8 kit. Briefly, the cells were cultured in 96-well plates (5×10^3 cells/well) for 24 h. Procyanidin capsules were then added at concentrations of 0.01, 0.03, 0.06, 0.12, 0.25, and 0.5 mg/mL and incubated for 24 or 48 h. CCK-8 reagent (10 μL) was added and incubated for ~ 2 h. Then the absorbance was measured at 450 nm using a spectrophotometer. Cell internalization was evaluated by CLSM. RAW 264.7 and DC2.4 cells were cultured in 24-well plates (5×10^4 cells/well) for 24 h, then 120 μg/mL procyanidin capsules were added and incubated for 24 h. The cells were fixed with 4 % paraformaldehyde for 10 min, permeabilized with 0.5 % Triton X-100, then stained with rhodamine phalloidin for 60 min following another 10 min DAPI staining before observation.

To evaluate the biocompatibility of the capsules *in vivo*, a wound was made on the backs of C57BL/6 mice, and then treated with 25 mg/kg capsules. Controls were treated with 0.9 % NaCl. After 7 days, the mice were sacrificed and the major organs (heart, liver, spleen, lung, and kidney) were collected for hematoxylin and eosin (H&E) staining.

2.5. Intracellular H_2O_2 scavenging assay

RAW 264.7 cells were cultured in DMEM containing 10 % FBS and 1 % penicillin streptomycin. DC2.4 cells were cultured in RPMI 1640 containing 10 % FBS and 1 % penicillin streptomycin. All cells were incubated in a CO2 incubator at 37 °C. RAW 264.7 and DC2.4 cells were cultured in 96-well plates (5×10^3 cells/well) for 24 h, and then treated with 0.12, 0.25, and 0.5 mg/mL capsules. After 12 h (RAW 264.7) and 24 h (DC2.4) treatment, the medium was replaced with medium containing 0.5 mM H_2O_2 and incubated for 30 min. The medium was replaced with fresh medium and incubated for 24 h, then assayed with CCK-8 reagent. Samples treated with 0.5 mM H_2O_2 alone served as the control.

2.6. Intracellular ROS assay

Intracellular ROS levels were measured by 2′,7′-dichloroflurescein diacetate (DCF-DA) assays in RAW 264.7 and DC2.4 cells. The cells were cultured in 24-well plates (5×10^4 cells/well) for 24 h, then 500 μg/mL H_2O_2 was added for about 30 min before replacing the medium with fresh medium containing procyanidin capsules (500 μg/mL). After incubation for another 24 h, DCF-DA (10 μM) was added for 30 min. Lastly, the cells were washed with culture medium and stained with DAPI before CLSM visualization and fluorescence quantitation using ImageJ.

2.7. Cell migration

DC2.4 cell migration was measured by scratch wound assay. Briefly, DC2.4 cells were cultured in 6-well plates (1×10^6 cells/well) and incubated for 24 h, then divided into four groups: the control group, the H_2O_2 group, the capsules group and the H_2O_2 plus capsules group. The H_2O_2 group and H_2O_2 plus capsules group were treated with 500 μg/mL H_2O_2 for 30 min, while the control and capsules groups were subject to treatment with fresh medium. A wound was artificially created on the cell monolayers by utilizing a 200 μL pipette tip to scratch them, suspended cells and debris were removed with PBS before adding fresh DMEM or DMEM-capsules. Wound area was measured at 0 h and 24 h under an optical microscope and the degree of scratch closure was calculated. The migration ratio was quantified using ImageJ software (National Institutes of Health, Bethesda, MD) and calculated as % Cell migration $= (S_0 - S_t)/S_0 \times 100$ %, where S_0 is the scratch area at 0 h and S_t is the scratch area remaining at 24 h.

2.8. Osteoarthritis model establishment and treatment

C57BL/6 mice (six weeks, male, ~20 g) were anesthetized with 0.3 % sodium pentobarbital for abdominal anesthesia (mg/kg). The OA model was established by removing the medial meniscus of the knees by quick resection, and then the wound was closed with absorbable sutures. 24 mice were randomly divided into four groups (six mice per group) as follows: the normal group (20 μL 0.9 % NaCl), the sham group (medial meniscectomy, and 20 μL 0.9 % NaCl), the PC group (medial meniscectomy and 20 μL PC solution (10 mg/kg), and the capsules group (medial meniscectomy and 20 μL sphere capsules (10 mg/kg). All groups were treated once after surgery, all mice were euthanized 4 weeks after surgery, and knees were collected for H&E staining.

2.9. Diabetic wounds model establishment and treatment

The diabetic wounds model was established in previous reports [26,27]. C57BL/6 mice were intraperitoneally injected with 100 mg/kg streptozotocin (STZ, Sigma-Aldrich) for 7 consecutive days and fed a normal diet. Glucose levels were monitored daily with a glucose meter. Mice with sustained blood glucose levels >250 mg/dL were considered as diabetes. About 2 weeks after initiation of STZ, the diabetic mice were anesthetized with 0.3 % sodium pentobarbital and a full-thickness cutaneous wound model was created. The backs of the mice were depilated, and full-thickness wounds (diameter 8 mm) were applied. The treatment groups were the same as described above. Mice were euthanized after 14 days and skin samples 8 mm around the wounds were collected for H&E staining.

2.10. Transcriptome analysis

Trizol reagent was used to extract total RNA from samples obtained from each *in vivo* model. Dynabeads Oligo (dT) (Thermo Fisher, CA, USA) were used in two rounds of purification to extract mRNA from total RNA. We performed 2 × 150-bp paired-end sequencing (PE150) on an Illumina Novaseq™ 6000 sequencer (LC-Bio Technology, Hangzhou, China) according to manufacturer protocols. Reads were aligned to the *Mus musculus* reference genome using HISAT2 after filtering with Cutadapt. Expression levels of all transcripts and the FPKM (fragment per kilobase of transcript per million mapped reads) value were obtained using StringTie and Ballgown [28]. Differential expression analysis between groups was performed with DESeq2 software, and the standard for differentially expressed genes was a false discovery rate below <0.05 and absolute fold change ≥2 [29]. Differentially expressed genes were analyzed for GO functions and KEGG pathway enrichment analysis [30]. The gene set enrichment analysis (GSEA) was utilized to assess the enrichment of two chronic inflammatory models in the KEGG pathway gene sets from a comprehensive standpoint (NES>1, NOM p-value< 0.05 and FDR q-value <0.25) [31]. STRING database (https://string-db.org/, version 12.0) collaborates with cytoscape in the construction and topology analysis of PPI networks [32,33]. MCODE plugin [34] is utilized to calculate the PPI subnetwork which is marked in yellow.

2.11. qRT-PCR validation

The mRNA expression of Lep, Pck1, Prkaa2 and GAPDH were examined by qRT-PCR validation analysis. The total RNA was extracted by employing an RNAsimple Total RNA Kit (TianGen, Beijing, China), and the extraction protocol was carefully followed to ensure optimal quality control. Thermal Cycler (BioRad, USA) was used to conduct reverse transcription. Quantitative reverse-transcription polymerase chain reaction (qRT-PCR) reactions were executed and subsequently analyzed utilizing a 7500 Fast Real-Time PCR System (Applied Biosystems, Foster City, CA) based on the comparative cycle threshold (Ct) (2-ΔΔCt) method.

2.12. Western blot

Post-maturation, Raw 247.6 cells were exposed to 500 μg/mL H_2O_2 for approximately 3 h, followed by a 24 h incubation with 500 μg/mL procyanidin capsules. Prepare the protein extraction solution in accordance with the standardized ratio of RIPA 1 mL to PMSF 10 μL. Concurrently, set forth the necessary materials required, such as the SDS loading buffer and other essential reagents. Following PBS-mediated cell washing, the cells were transferred to a pre-cooled cracking working fluid ice bath for a duration of 10 min. Subsequently, the cells were removed using a cell scraper and transferred to a centrifuge tube for further cracking in the same ice bath for 5–10 min. Once cracking was deemed complete, the cells were centrifuged at a speed of 12000g at a temperature of 4 °C for a duration of 5 min. The concentration of protein in supernatant was measured by BCA kit. Add the corresponding volume of SDS loading buffer to the supernatant, boiling water denaturation. The protein sample was electrophoretically separated using a 12 % polyacrylamide gel and subsequently transferred to a PVDF membrane using a wet transfer methodology. The membrane was then sealed using a 5 % skim milk background and incubated with the corresponding primary antibodies against Pck1, Prkaa2, and GAPDH overnight at an appropriate temperature. Subsequently, the membrane was incubated with secondary antibodies for 1.5 h. Then, the membrane was processed for color development and visualization to determine the relative expression abundance.

2.13. Statistical analysis

All quantitative data are presented as the mean ± standard error (SE). Statistical comparisons amongst groups were performed utilizing one-way ANOVA, with subsequent analysis conducted via Tukey's test (GraphPad Prism 5, GraphPad Software, San Diego, USA). Significant differences were categorized as meeting a predetermined minimal significance level of $p < 0.05$, and denoted * $p < 0.05$, ** $p < 0.01$, *** $p < 0.001$, and **** $p < 0.0001$.

3. Results and discussion

3.1. Preparation of procyanidin capsules

Microcapsules are promising long-acting biomaterials with excellent stable physicochemical characteristics and nanostructure [35], hence we selected microcapsules to achieve long-term ROS scavenging ability. Procyanidin (PC) was incubated with the $CaCO_3$ template to obtain procyanidin capsules after removing the $CaCO_3$. Optical microscopy revealed transparent circles, indicating that the procyanidin capsules were spherical and uniformly dispersed in solution (Fig. 2A). CLSM imaging of pure water and procyanidin solutions showed that the PC solution was a clear green (Fig. S1A), while the pure water was colorless (Fig. S1B), so the green circles depicted within the CLSM image confirmed successful capsules formation (Fig. 2B). The SEM images in Fig. 2C revealed a collapsed morphology, with folds and creases, and the capsules were approximately 3 μm (Fig. 2D). Permeability of the procyanidin capsules was investigated by incubation with FITC-dextran of different molecular weights (Fig. 2E). CLSM images show that the procyanidin capsules were permeable to FITC-dextran 40 kDa (Fig. 2E1) and impermeable to FITC-dextran 500 kDa (Fig. 2E2), suggesting that the capsules can transport drugs with molecular weights greater than 40 kDa. Furthermore, stability was also tested by storing procyanidin capsules in pure water, PBS, 0.9 % NaCl, and DMEM for 9 days. SEM imaging showed that the capsules retained the morphology and were thus stable in all solutions, particularly in 0.9 % NaCl solution, which was amenable for further *in vivo* and *in vitro* experimentation (Fig. 2F).

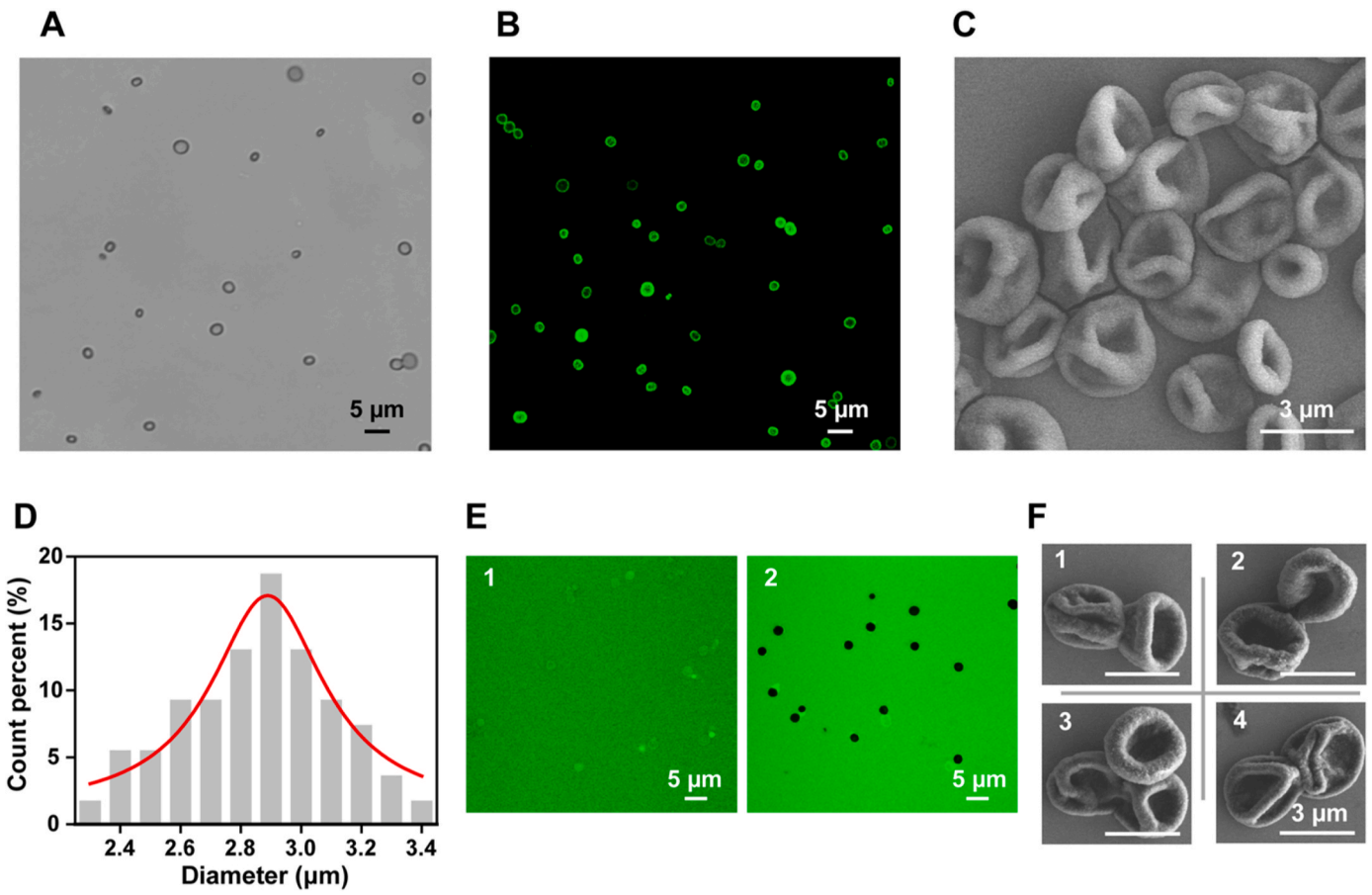

Fig. 2. The preparation behavior of procyanidin capsules. (A) OM, (B) CLSM and (C) SEM images of procyanidin capsules. (D) The size distribution of procyanidin capsules by SEM images. (E) CLSM images of procyanidin capsules against FITC dextran with Mw of (1) 40 kDa and (2) 500 kDa. The scale bars in (1) and (2) are 5 μm. (F) Stability of capsules in the solution of (1) pure water, (2) PBS solution, (3) 0.9 % NaCl and (4) DMEM. The scale bars in (A), (B) and (E) are 5 μm, in (C) and (F) are 3 μm.

3.2. Characterization and ROS scavenging assay of procyanidin capsules

The formation of procyanidin capsules was investigated by FTIR spectra, which showed the absorbance band of PC and the capsules always appeared as two absorbance bands at 1500-1600 cm^{-1} and 1600-1670 cm^{-1} representing C=C stretching vibrations of the benzene ring (Fig. 3A) [36]. The absorbance band of capsules near 1690 cm^{-1} represented carbonyl groups of amides, indicating the high degree of similarity between PC and capsule structures [37]. XPS spectra indicated the presence of carbon elements (66.56 %), oxygen elements (33.41 %) and calcium element (0.03 %) in the capsules (Fig. 3B and C). The plasma-mass spectrometry (ICP-MS) was used to detect the presence of calcium ions in the capsules and the results indicated that the procyanidin capsules were composed of procyanidin and did not contain calcium (Fig. S2). To further investigate the mechanism of capsules formation, we incubated the procyanidin solution with $CaCO_3$ for 12 h, 48 h, and 72 h to observe changes in the formed capsules (Fig. 3D). The capsules wall became thicker over time. At 48 h, spherical capsules started to form, and they were abundant at 72 h. To examine the structure, the spherical capsules were ultrasonicated for 10 min to destroy the structure and imaged by SEM, which showed the capsules were partially disrupted (Fig. 3E). The disrupted areas were enlarged to reveal that the interior of the capsules was not hollow but more like a dense network (Fig. 3F).

We speculate that the mechanism underlying procyanidin capsules formation involves the initial adsorption of PC onto the $CaCO_3$ template followed by progressive penetration of PC into the template interior as incubation time is extended. When HCl is added, the $CaCO_3$ dissolves away and the deposited procyanidin instantly forms a cross-linked network. The capsules are a multilayered cross-linked network with walls that thicken and pores that shrink with extended adsorption time. When the procyanidin adsorption time is sufficiently long, spherical capsules form, most likely due to the dense internal cross-linked network allowing the capsules to remain spherical rather than collapsing under dry conditions. Polystyrene microspheres and silica spheres were used as templates to explore the universality of this method of preparing procyanidin capsules (Fig. 3G). The procyanidin solution was incubated with the two templates for 72 h, then procyanidin capsules were synthesized by using tetrahydrofuran to remove the polystyrene microspheres templates and using hydrofluoric acid to remove the silica templates, respectively (Fig. 3G). SEM images confirmed the successful synthesis of capsules utilizing polystyrene microspheres and silica spheres as templates. This demonstrated that the preparation method is not limited to $CaCO_3$ templates, thereby making the method of preparing procyanidin capsules universally applicable.

FRAP assay detects the change of oxidized ferric ions to ferrous ions to estimate total ROS scavenging capacity [38]. The DPPH assay detects the change of free DPPH radicals to stable DPPH molecules to specifically evaluate radical scavenging ability [39]. The FOX assay detects the purple product formed when xylenol orange binds ferric ions to specifically evaluate hydrogen peroxide (H_2O_2) scavenging ability [40]. These three methods were employed to assess the ROS scavenging ability of procyanidin capsules in a systematic manner. Vitamin C (Vc), PC solution, and capsules were placed at room temperature in an oxygenated environment for one day, the free radical scavenging ability, H_2O_2 scavenging ability and DPPH radical scavenging ability of Vc, PC

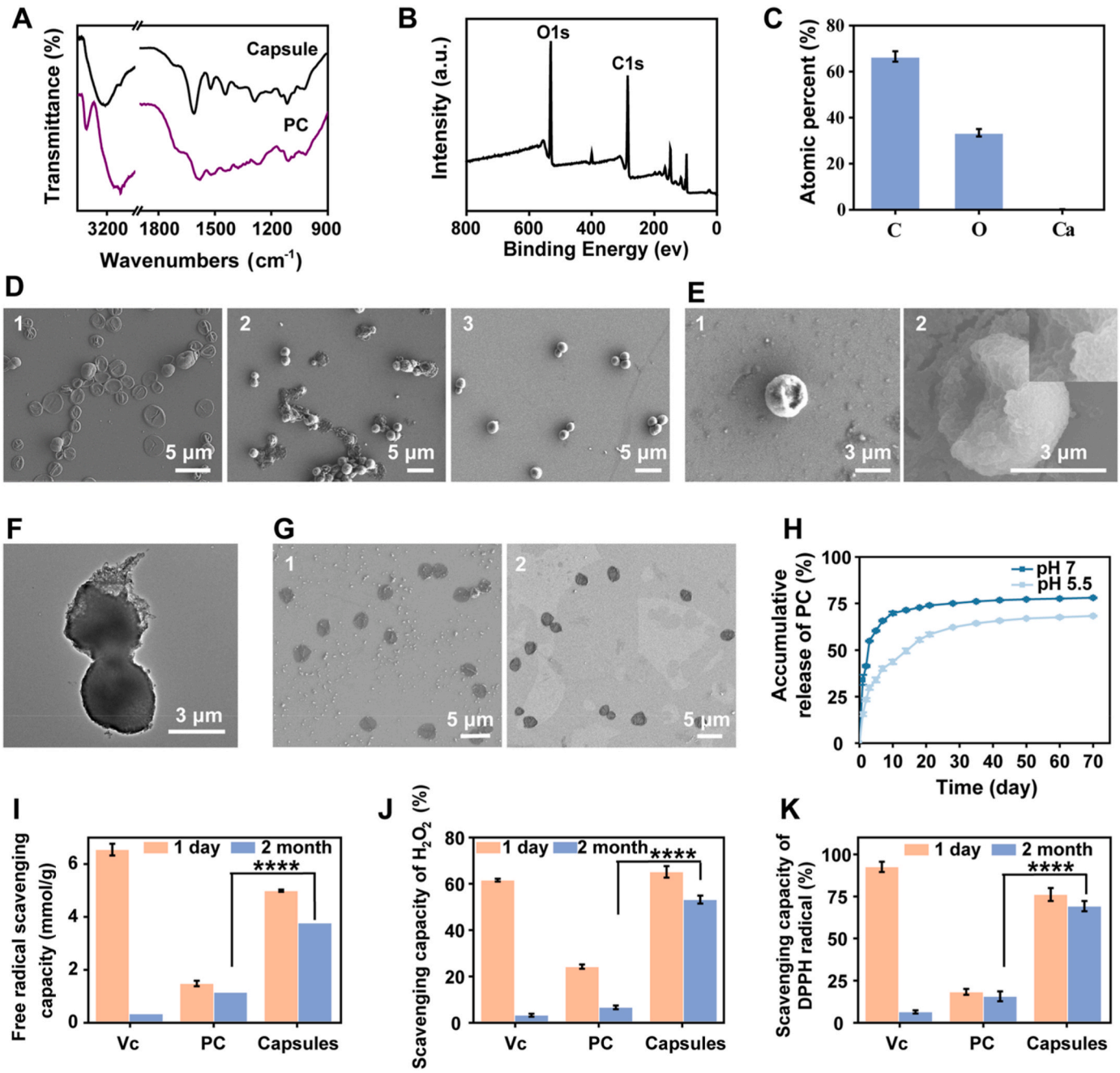

Fig. 3. The characterization and ROS scavenging assay of procyanidin capsules. (A) FTIR spectra of PC and procyanidin capsules. (B) XPS spectra of procyanidin capsules. (C) The element percentage of PC capsules by XPS spectra. (D) SEM images of procyanidin capsules which were prepared by incubating PC and $CaCO_3$ for about (1) 12 h, (2) 48 h, and (3) 72 h. Scale bars: 5 μm. (E) (1) SEM images of procyanidin capsules which were prepared by incubating PC and $CaCO_3$ for three days and sonicated for 10 min under ultrasonic conditions. (2) The magnified image of (1). Scale bars: 3 μm. (F) TEM image of procyanidin capsules which were prepared by incubating PC and $CaCO_3$ for three days and sonicated for 10 min under ultrasonic conditions. Scale bars: 3 μm. (G) SEM images of procyanidin capsules which were prepared by incubating PC with (1) PS templates, and (2) SiO_2 templates for 12 h. Scale bars: 5 μm. (H) The accumulative release curves of PC by procyanidin capsules at pH 7.4 and 5.5 *in vitro*. (I) Free radical scavenging ability, (J) H_2O_2 scavenging ability and (K) DPPH radical scavenging ability of Vc, PC and capsules. The data on the left of VC, PC and procyanidin capsules in (H), (I) and (J) represent short-term ROS scavenging ability (1 day), and the right represents the long-term scavenging ability (2 month). (P values: ****$P < 0.0001$, all the values are expressed as mean ± SD, n = 3).

and capsules were similar, indicating that the capsules had good ROS scavenging ability (Fig. 3I–K, left). The scavenging effects of the procyanidin capsules on superoxide anions and ABTS free radicals were 3.79 and 1.67 times higher than the PC solution, and the superoxide anion-scavenging ability was even higher than Vc (Fig. S3). Then, we evaluated the long-term ROS scavenging ability of Vc, PC, and capsules after room temperature storage for 2 months. the free radical scavenging ability, H_2O_2 scavenging ability and DPPH radical scavenging ability of procyanidin capsules were 13.22, 20.14, and 12.36 times higher than those of Vc (Fig. 3I–K, right). The results showed that the capsules structure formed by PC is more stable, and procyanidin capsules can exert ROS scavenging ability for a longer period of time than Vc or PC.

To explore the mechanisms behind the long-lasting ROS scavenging effect of procyanidin capsules, we carried out an in-depth study on the manner in which these capsules release PC. Notably, PC can be released slowly by procyanidin capsules for up to 70 days under physiological pH

7.4 conditions, and this release process was much slower at a lower pH 5.5 (Fig. 3H). Lysosomes perform key functions such as secretion, cell signaling, plasma membrane repair, and energy metabolism. Typically, cells uptake capsules through endocytosis and then transport them to the lysosomes for specialized functions [41,42]. Lysosomal enzymes such as the vacuolar-type ATPase (V-ATPase) established an electrochemical gradient to maintain a low acidic pH environment in lysosomes [43,44]. Upon endocytosis, cargo molecules such as procyanidin capsules undergo slow disassembly and release PC within this acidic environment [45]. Fig. 3H showed that PC was obviously released slower by

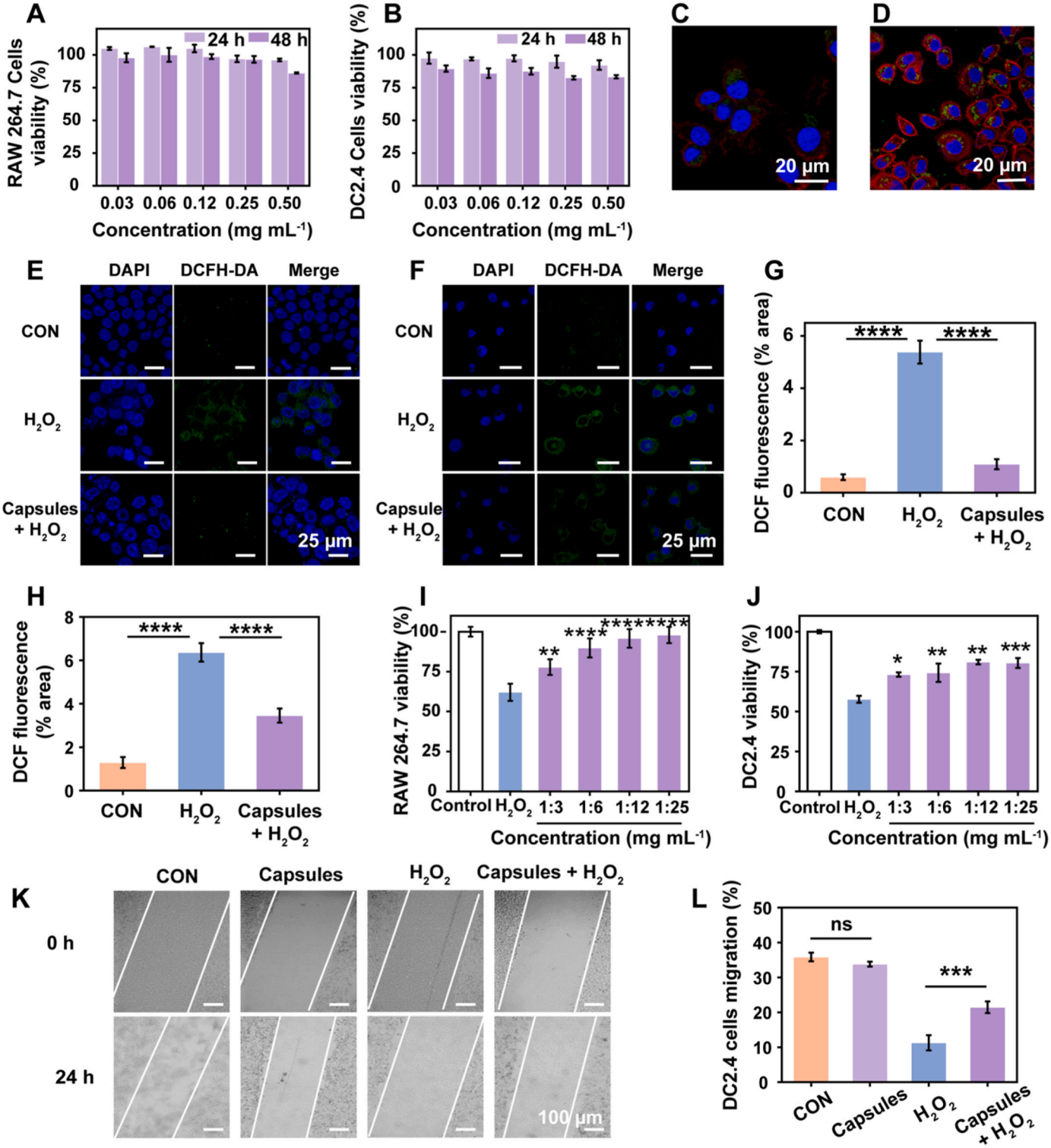

Fig. 4. Procyanidin capsules safely and effectively eliminate intracellular ROS. Cell viability of (A) RAW 264.7 cells and (B) DC2.4 cells. Cellular uptake of capsules in (C) RAW 264.7 and (D) DC2.4 cells. Scale bars: 20 μm. CLSM images of ROS scavenging in (E) RAW 264.7 and (F) DC2.4 cells using DCFH-DA probe (50 μg mL^{-1}). Scale bars: 25 μm. (G) RAW 264.7 and (H) DC2.4 cells of DCFH-DA probe by DCF fluorescence through CLSM images. (I) RAW 264.7 cells viability induced by H_2O_2. (J) DC2.4 cells viability induced by H_2O_2. (K) Digital images of DC2.4 cells migration of scratch assay. Scale bars: 100 μm. (L) Quantification of DC2.4 cells migration. (P values: *P < 0.05, **P < 0.01, ***P < 0.001, ****P < 0.0001, all the values are expressed as mean ± SD, n = 3).

procyanidin capsules under lower pH conditions that mimic lysosomes *in vitro*. We propose that procyanidin capsules could effectively long-term scavenge ROS by gradually releasing PC within the acidic lysosomal environment after endocytosis.

3.3. Procyanidin capsules scavenge intracellular ROS safely and effectively

The cytotoxicity of procyanidin capsules was evaluated by CCK-8 assay, which showed the cell viability of both RAW 264.7 and DC2.4 was higher than 90 % at different concentrations of procyanidin capsules for 24 h (Fig. 4A and B). Even treated with high concentration procyanidin capsules (500 μg/mL) for 48 h, the viability of two cells remained >80 %. The results indicated extremely low cytotoxicity and good biocompatibility of procyanidin capsules which was consistent with our previous findings [46]. To evaluate the intracellular distribution, procyanidin capsules incubated with RAW 264.7 and DC2.4 for 24 h were imaged by CLSM. The uptake green capsules were largely located in the cytoplasm and were not observed in other organelles, including the cell membrane (red) and nucleus (blue) (Fig. 4C and D). The commonly used intracellular ROS green fluorescent probe DCFH-DA was utilized to assess the scavenging ability of procyanidin capsules in the previous two cell lines. As shown in Fig. 4E and F, cytoplasmic ROS induced by H_2O_2 was reduced by procyanidin capsules from 5.38×10^3 to 1.09×10^3 in RAW 264.7 and from 6.36×10^3 to 3.46×10^3 in DC2.4 (Fig. 4G and H). Consistently, the viability of RAW 264.7 and DC2.4 was significantly improved by procyanidin capsules compared to the H_2O_2 group (Fig. 4I and J). Moreover, the migration of DC2.4 cells was significantly suppressed by hydrogen peroxide and partially rescued by procyanidin capsules (Fig. 4K and L). The results confirmed procyanidin capsules exhibited minimal toxicity and side effects on cellular function, and could effectively eliminate ROS in cells.

3.4. Long-term ROS scavenging ability of procyanidin capsules in osteoarthritis and diabetic wounds

To evaluate the long-term ROS scavenging ability of procyanidin capsules *in vivo*, osteoarthritis and diabetic wound models were built and treated with procyanidin capsules. In the osteoarthritis model, procyanidin capsules ameliorated the synovial membrane degeneration induced by surgery (Fig. 5A). Quantitative polymerase chain reaction analysis of IL-6 and TNF-α in the joint showed decreases of 10 % and 36 % (PC) and 78 % (procyanidin capsules) compared to the control (Fig. S4). In diabetic wounds model, procyanidin capsules accelerated skin wound healing from 3 to 14 days compared to the control (Fig. 5B). Histological analysis of 14 days impaired skin regions revealed that the length of the undetached scabbed regions of procyanidin capsules group was visibly shorter than the control group or the PC treated group (Fig. 5C). The IL-6 and TNF-α in the wound sections were showed by immunohistochemical staining (Fig. 5D) and quantitative analyses showed the two levels were decreased in the capsules group compared to the control or PC group (Fig. 5E and F). Furthermore, the biosafety of procyanidin capsules was assessed through H&E staining that showed no significant alteration in the heart, liver, spleen, lung, and kidney after the capsules treatment (Fig. 5G). The results showed that procyanidin capsules can safely and effectively alleviate symptoms of two representative and chronic types of inflammation *in vivo*.

3.5. The AMP-activated protein kinase (AMPK) signaling was identified as the common signaling regulated by procyanidin capsules in osteoarthritis and diabetic wounds

We utilized transcriptome to investigate ROS scavenging related DEGs regulated by procyanidin capsules in osteoarthritis or diabetic wounds. After mapping clean reads to the *Mus musculus* reference genome, 309 DEGs (222 up-regulated and 87 down-regulated) were figured out in osteoarthritis, while 79 DEGs (59 up-regulated and 20 down-regulated) were detected in diabetic wounds (Fig. 6A and B). GO enrichment analysis of osteoarthritis revealed large amounts of DEGs in the biology process cluster in immune function, and in the cellular component the expression of myosin-related genes were substantially observed, with the expression of myosin heavy polypeptide 8 (Myh8), actinin alpha 3 (Actn3) and myosin binding protein C (Mybpc2) was significantly up-regulated by procyanidin capsules (Fig. 6C). Previous studies have shown crocin [47] or baicalin [48] could alleviate osteoarthritis accompanied by increasing the expression of myosin heavy chain IIa. In diabetic wounds we found the enrichment of the complement activation and the membrane attack complex (Fig. 6D). The complement system, which is a critical component of our innate immune system, plays a pivotal role in protecting the body from foreign invaders [49]. The membrane attack complex serves as an integral part of the immune system's swift and efficient first line of defense and soluble complement proteins C5b, C6, C7, C8, and C9 form the complex by sequential assembly [50,51].

Further Kyoto Encyclopedia of Genes and Genomes (KEGG) enrichment analysis showed peroxisome proliferator-activated receptor (PPAR), NF-kappa B (NF-κB), cytokine-cytokine receptor interaction and AMP-activated protein kinase (AMPK) signalings were significantly enriched in osteoarthritis (Fig. 6E). In diabetic wounds, glucagon, insulin and AMPK signalings were significantly enriched (Fig. 6F). AMPK emerged as a common and substantial enrichment signaling in both osteoarthritis and diabetic wounds regulated by procyanidin capsules. Gene Set Enrichment Analysis (GSEA) can discern whether a given set of genes is significantly enriched in one of two distinct biological states from a global view [31]. GSEA data further confirmed that the AMPK signaling was significantly up-regulated in both two models, with 25 leading core enrichment genes in osteoarthritis or 45 core genes in diabetic wounds, and 18 common core genes shared by the two models (Fig. 6G and H). Taken together, the above data suggested that AMPK signaling was the most commonly regulated signaling by procyanidin capsules in osteoarthritis and diabetic wounds.

3.6. The molecular network of the key AMPK signaling members regulated by procyanidin capsules

Aberrant mitochondrial activation is a major source of excessive ROS, and activation of AMPK signaling inhibits mitochondrial activation to scavenge ROS [52]. The previous results confirmed the ability of procyanidin capsules to scavenge ROS *in vitro* and *in vivo* (Figs. 4 and 5). Here we constructed a protein-protein interaction (PPI) network of DEGs from osteoarthritis and diabetic wounds based on STRING database and visualized by cytoscape to characterize the molecular network regulated by procyanidin capsules. The yellow marked nodes representing DEGs of the AMPK signaling formed the important parts of the network (Fig. 7A and B), and the results further confirm that the AMPK signaling was an important molecular signal co-regulated by procyanidin capsules in osteoarthritis and diabetic wounds (Fig. 6).

In addition to phosphoenolpyruvate carboxykinase 1 (Pck1) and leptin (Lep) which were shared by the AMPK signaling in two networks, we also discovered AMP-activated catalytic subunit alpha 2 (Prkaa2) was significantly up-regulated in osteoarthritis (1.66-fold change) or diabetic wounds (1.99-fold change) with both q-value less than 0.01. Then we detected the protein expression of the three common members from the AMPK signaling in osteoarthritis and diabetic wounds. Compared to normal chondrocytes, AMPK phosphorylation levels were significantly lower in osteoarthritis chondrocytes [53]. Activation of AMPK, a crucial regulator of glucose homeostasis, has been identified as a promising therapeutic approach for treating type 2 diabetes mellitus and other related metabolic disorders [54]. Lep enhances the development of osteoarthritis by acting on the cartilage, inducing both pro-inflammatory and pro-catabolic effects [55]. Our results indicate that besides down-regulating expression of Lep in osteoarthritis,

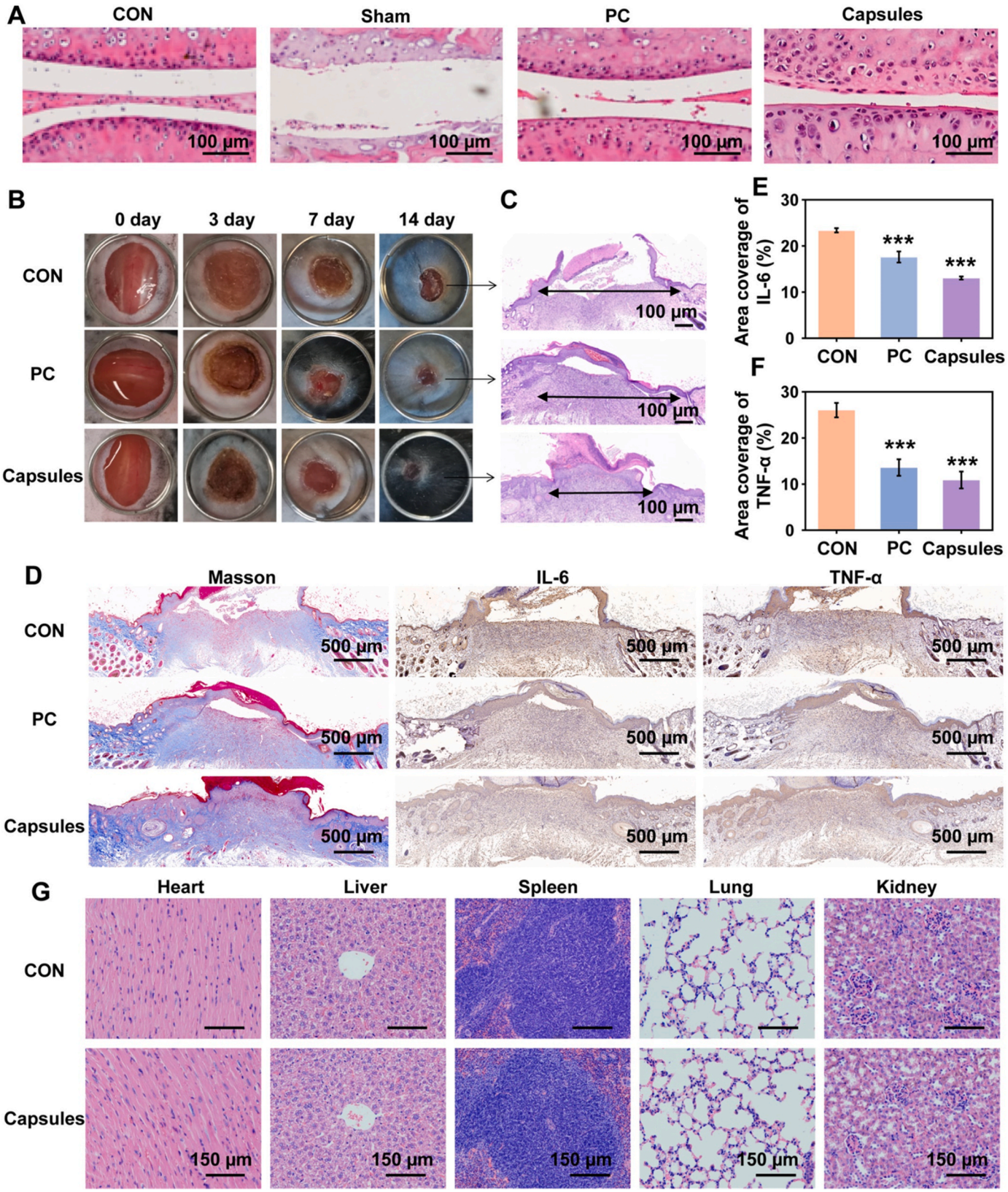

Fig. 5. Procyanidin capsules significantly improved osteoarthritis and diabetic wounds. (A) H&E staining of osteoarthritis. Scale bars: 100 μm. (B) The digital imageof skin wounds treated with PBS as control, PC and procyanidin capsules in diabetic wounds model. (C) The H&E staining sections of skin wounds treated with PBS as control, PC and procyanidin capsules in diabetic wounds model. Scale bars: 100 μm. (D) Masson's trichrome staining and immunohistochemical IL-6 and TNF-α staining of wound sections of the granulation tissue on the 14 day. Scale bars: 500 μm. (E) Quantification of immunohistochemical IL-6 staining. (F) Quantification of immunohistochemical TNF-α staining. (G) H&E staining of normal tissues including heart, liver, spleen, lung and kidney of mice after treatments. Scale bars: 100 μm. The magnifications of all images were 200 × . (P values: ***$P < 0.001$, all the values are expressed as mean ± SD, n = 3).

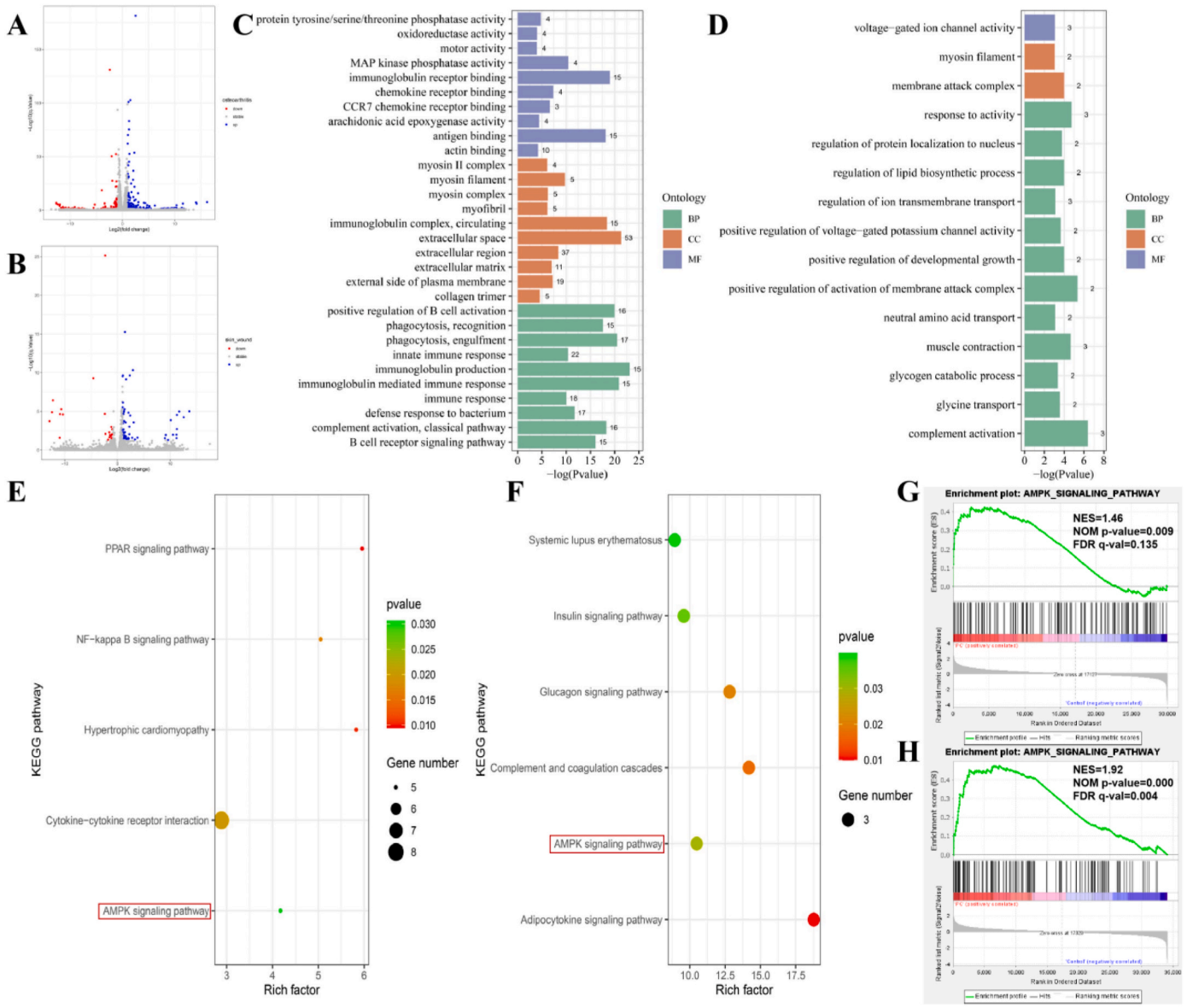

Fig. 6. Transcriptome landscape of DEGs regulated by procyanidin capsules. Volcano plot displaying DEGs between procyanidin capsules and the control group in osteoarthritis model (A) and diabetic wounds (B). GO enrichment analysis of DEGs in osteoarthritis (C) and diabetic wounds (D). KEGG enrichment analysis of DEGs in osteoarthritis (E) and diabetic wounds (F). GSEA analysis of AMPK signaling gene set in osteoarthritis (G) and diabetic wounds (H).

procyanidin capsules boosted the expression of Pck1 and Prkaa2 in osteoarthritis (Fig. 7C), and promoted the expression of Pck1, Lep and Prkaa2 in diabetic wounds (Fig. 7D). Several studies have shown that the increase of Pck1 and Prkaa2 expression in osteoarthritis can lead to a positive effect on the disease [53,56], our results suggested that the improvement of osteoarthritis by procyanidin capsules may be due to the up-regulation of Pck1 and Prkaa2 (Figs. 5A and 7C). In diabetic mice, over-expression of Pck1 and Prkaa2 can improve diabetic nephropathy [57] and diabetic cardiomyopathy [58], and high levels of Lep can inhibit hyperglycemia [59]. Through transcriptome and qRT-PCR validation, we demonstrated that procyanidin capsules commonly up-regulated three AMPK signaling members to improve diabetic wounds (Figs. 5B and 7D).

AMPK activity and ROS production are highly interconnected, as ROS production largely depends on the activity of mitochondria [52]. The transcriptomes and WB of two chronic inflammatory have demonstrated that procyanidin capsules can activate AMPK signaling to improve inflammatory damage. Previously, we validated that the procyanidin capsules can notably decrease the intracellular ROS levels in RAW 264.7 and DC2.4 cell lines by green fluorescent probe DCFH-DA (Fig. 4G and H). Here, we observed the expression of Pck1 and Prkaa2, crucial genes of the AMPK signaling, in RAW 264.7 cells. Significantly decreased levels of the gene and protein expressions of Pck1 and Prkaa2 were observed in RAW 264.7 cells treated with H_2O_2 when compared with control cells. The expression of Pck1 and Prkaa2 increased considerably in cells that were supplemented with procyanidin capsules (Fig. 7E–G). It can be seen that the intracellular ROS levels are negatively correlated with the expression levels of Pck1 and Prkaa2. Our results suggest that procyanidin capsules can scavenge ROS by activating AMPK signaling and exert long-lasting anti-inflammatory effects in osteoarthritis and diabetic wounds (Fig. 7G). These effects can be achieved with a single treatment, and does not result in significant pathological damage to various organs (Fig. 5G).

4. Conclusion

In conclusion, the present study has successfully developed a simple method for production of procyanidin capsules. The prepared

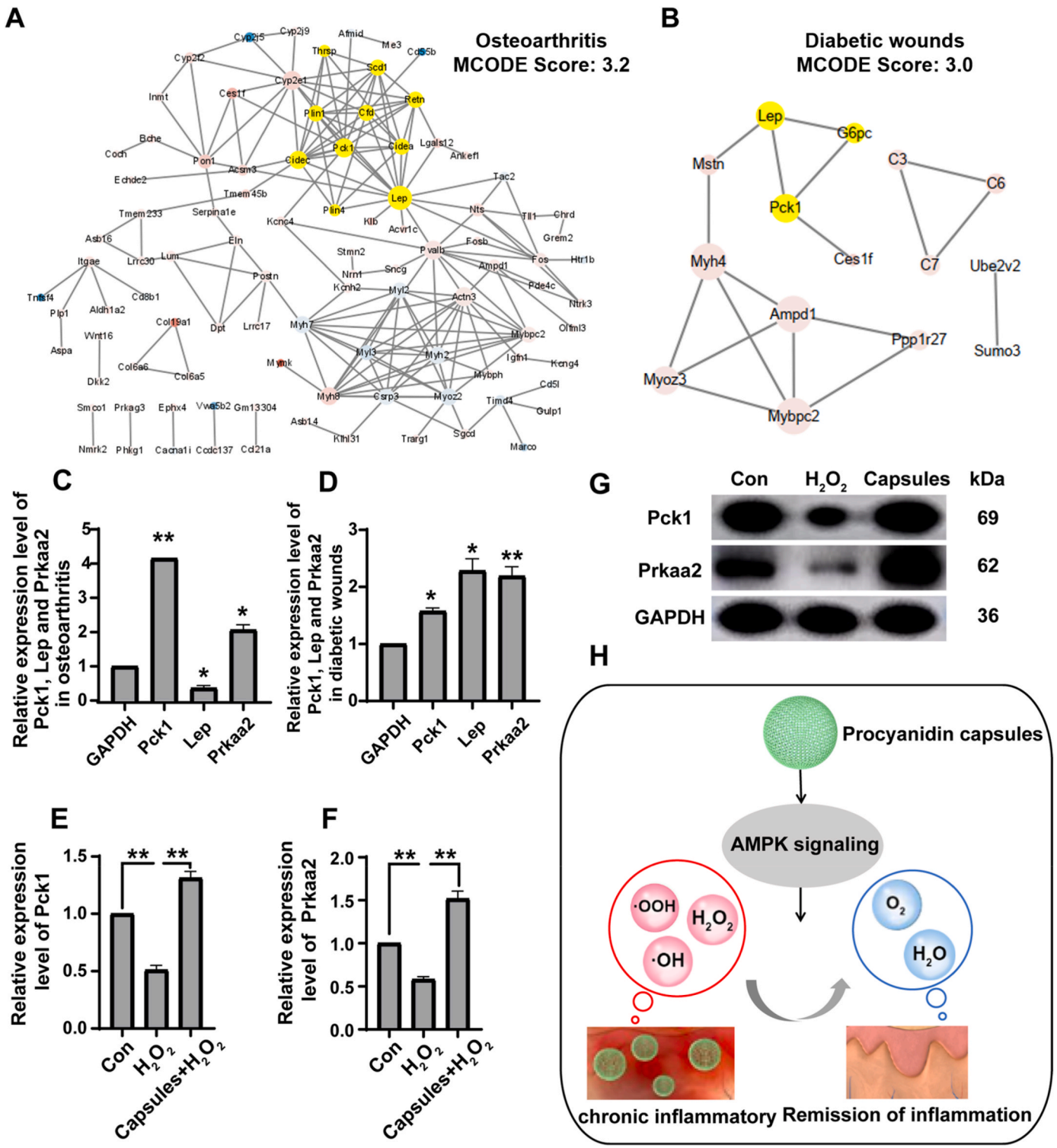

Fig. 7. Procyanidin capsules activate AMPK signaling. PPI network of DEGs in osteoarthritis (A) and diabetic wounds (B). The size of the node is positively correlated with the degree, blue indicates down-regulated expression, while red signifies up-regulated expression. The yellow highlighted area is the MCODE subnet. (C) Relative expression of Pck1, Lep and Prkaa2 were examined by qRT-PCR in osteoarthritis. (D) Relative expression of Pck1, Lep and Prkaa2 were examined by qRT-PCR in diabetic wounds. (E) Relative expression of Pck1 was examined by qRT-PCR in H_2O_2 and Capsules + H_2O_2 treatment RAW 264.7 cells. (F) Relative expression of Prkaa2 was examined by qRT-PCR in H_2O_2 and Capsules + H_2O_2 treatment RAW 264.7 cells. (G) Representative WB bands of Pck1 and Prkaa2 in H_2O_2 and Capsules + H_2O_2 treated RAW 264.7 cells. (H) Procyanidin capsules scavenge ROS via AMPK activation for long-lasting anti-inflammatory effects. (P values: *$P < 0.05$, **$P < 0.01$, all the values are expressed as mean ± SD, n = 3).

procyanidin capsules demonstrated remarkable chemical stability, enabling them to efficiently scavenge excessive ROS through slow-release procyanidin. Furthermore, procyanidin capsules exhibited promising therapeutic efficacy in osteoarthritis and diabetic wounds. These results suggest that procyanidin capsules could be a promising candidate for the treatment of chronic inflammatory diseases. As such, future research efforts will focus on exploring the feasibility of employing similar or alternative methodologies for the synthesis of other polyphenolic biomaterials and evaluating the effectiveness of these constructed polyphenolic biomaterials in mitigating chronic inflammatory diseases.

CRediT authorship contribution statement

Linxiao Sun: Writing – original draft, Visualization, Methodology, Funding acquisition, Formal analysis, Data curation, Conceptualization. **Shaoyin Wei:** Writing – original draft, Visualization, Methodology, Investigation, Formal analysis. **Chenglong Wang:** Methodology, Conceptualization. **Yipiao Zhang:** Writing – original draft, Conceptualization. **Xingjie Zan:** Writing – review & editing, Funding acquisition, Data curation, Conceptualization. **Lianxin Li:** Writing – review & editing, Funding acquisition, Conceptualization. **Chunwu Zhang:** Writing – review & editing, Resources, Project administration, Methodology.

Declaration of competing interest

All the authors of this paper declare that we have no known competing financial interests or personal relationships that could have appeared to influence the work reported in this paper. There is no professional or other personal interest of any nature or kind in any product, service or company that could be construed as influencing the position presented in, or the review of the manuscript entitled.

Acknowledgements

This work was financially supported by the One Thousand Talents Program, startup funding from the Wenzhou Institute of UCAS (WIUCASQD2019009), National Science Foundation of China (82104580) and Shandong Province Major Scientific and Technical Innovation Project (No. 2021SFGC0502).

Appendix A. Supplementary data

Supplementary data to this article can be found online at https://doi.org/10.1016/j.mtbio.2024.101310.

Data availability

Data will be made available on request.

References

[1] C. Nathan, Points of control in inflammation, Nature 420 (6917) (2002) 846–852.
[2] L. Ferrucci, E. Fabbri, Inflammageing: chronic inflammation in ageing, cardiovascular disease, and frailty, Nat. Rev. Cardiol. 15 (9) (2018) 505–522.
[3] D. Okin, R. Medzhitov, Evolution of inflammatory diseases, Curr. Biol. : CB 22 (17) (2012) R733–R740.
[4] K. Apel, H. Hirt, Reactive oxygen species: metabolism, oxidative stress, and signal transduction, Annu. Rev. Plant Biol. 55 (2004) 373–399.
[5] A. Harijith, D.L. Ebenezer, V. Natarajan, Reactive oxygen species at the crossroads of inflammasome and inflammation, Front. Physiol. 5 (2014) 352.
[6] V. Falanga, Wound healing and its impairment in the diabetic foot, Lancet (London, England) 366 (9498) (2005) 1736–1743.
[7] D. D'Amico, M. Olmer, A.M. Fouassier, P. Valdés, P.A. Andreux, C. Rinsch, M. Lotz, Urolithin A improves mitochondrial health, reduces cartilage degeneration, and alleviates pain in osteoarthritis, Aging Cell 21 (8) (2022) e13662.
[8] M. Mittal, M.R. Siddiqui, K. Tran, S.P. Reddy, A.B. Malik, Reactive oxygen species in inflammation and tissue injury, Antioxidants Redox Signal. 20 (7) (2014) 1126–1167.
[9] A. Dimozi, E. Mavrogonatou, A. Sklirou, D. Kletsas, Oxidative stress inhibits the proliferation, induces premature senescence and promotes a catabolic phenotype in human nucleus pulposus intervertebral disc cells, Eur. Cell. Mater. 30 (2015) 89–102. ; discussion 103.
[10] Y. Wang, K. Xia, L. Wang, M. Wu, X. Sang, K. Wan, X. Zhang, X. Liu, G. Wei, Peptide-engineered fluorescent nanomaterials: structure design, function tailoring, and biomedical applications, Small 17 (5) (2021) e2005578.
[11] D.K. Manna, P. Maity, A.K. Nandi, M. Pattanayak, B.C. Panda, A.K. Mandal, S. Tripathy, K. Acharya, A.K. Sahoo, N. Gupta, S. Roy, S.S. Islam, Structural elucidation and immunostimulating property of a novel polysaccharide extracted from an edible mushroom Lentinus fusipes, Carbohydr. Polym. 157 (2017) 1657–1665.
[12] X. Mu, H. He, J. Wang, W. Long, Q. Li, H. Liu, Y. Gao, L. Ouyang, Q. Ren, S. Sun, J. Wang, J. Yang, Q. Liu, Y. Sun, C. Liu, X.D. Zhang, W. Hu, Carbogenic nanozyme with ultrahigh reactive nitrogen species selectivity for traumatic brain injury, Nano Lett. 19 (7) (2019) 4527–4534.
[13] H. Yao, Y. Zhang, L. Liu, Y. Xu, X. Liu, J. Lin, W. Zhou, P. Wei, P. Jin, L.P. Wen, Inhibition of lanthanide nanocrystal-induced inflammasome activation in macrophages by a surface coating peptide through abrogation of ROS production and TRPM2-mediated Ca(2+) influx, Biomaterials 108 (2016) 143–156.
[14] X.W. Chen, X.Y. Sun, G.H. Tang, J.M. Ouyang, Sulfated Undaria pinnatifida polysaccharide inhibits the formation of kidney stones by inhibiting HK-2 cell damage and reducing the adhesion of nano-calcium oxalate crystals, Biomater. Adv. 134 (2022) 112564.
[15] K.Y. Sun, Y. Wu, J. Xu, W. Xiong, W. Xu, J. Li, Z. Sun, Z. Lv, X.S. Wu, Q. Jiang, H. L. Cai, D. Shi, Niobium carbide (MXene) reduces UHMWPE particle-induced osteolysis, Bioact. Mater. 8 (2022) 435–448.
[16] H.C. Hung, K.J. Joshipura, R. Jiang, F.B. Hu, D. Hunter, S.A. Smith-Warner, G. A. Colditz, B. Rosner, D. Spiegelman, W.C. Willett, Fruit and vegetable intake and risk of major chronic disease, J. Natl. Cancer Inst. 96 (21) (2004) 1577–1584.
[17] H. Boeing, A. Bechthold, A. Bub, S. Ellinger, D. Haller, A. Kroke, E. Leschik-Bonnet, M.J. Müller, H. Oberritter, M. Schulze, P. Stehle, B. Watzl, Critical review: vegetables and fruit in the prevention of chronic diseases, Eur. J. Nutr. 51 (6) (2012) 637–663.
[18] B. Hu, Y. Shi, C. Lu, H. Chen, Y. Zeng, J. Deng, L. Zhang, Q. Lin, W. Li, Y. Chen, F. Zhong, X. Xia, Raspberry polyphenols alleviate neurodegenerative diseases: through gut microbiota and ROS signals, Food Funct. 14 (17) (2023) 7760–7779.
[19] X. Zhao, X. Shi, Q. Liu, X. Li, Tea polyphenols alleviates acetochlor-induced apoptosis and necroptosis via ROS/MAPK/NF-κB signaling in Ctenopharyngodon idellus kidney cells, Aquat. Toxicol. 246 (2022) 106153.
[20] Z.R. Xu, J.Y. Li, X.W. Dong, Z.J. Tan, W.Z. Wu, Q.M. Xie, Y.M. Yang, Apple polyphenols decrease atherosclerosis and hepatic steatosis in ApoE-/- mice through the ROS/MAPK/NF-κB pathway, Nutrients 7 (8) (2015) 7085–7105.
[21] F.A. Tomás-Barberán, C. Andrés-Lacueva, Polyphenols and health: current state and progress, J. Agric. Food Chem. 60 (36) (2012) 8773–8775.
[22] C. Sandoval-Acuña, J. Ferreira, H. Speisky, Polyphenols and mitochondria: an update on their increasingly emerging ROS-scavenging independent actions, Arch. Biochem. Biophys. 559 (2014) 75–90.
[23] Z. Ni, H. Yu, L. Wang, Y. Huang, H. Lu, H. Zhou, Q. Liu, Multistage ROS-responsive and natural polyphenol-driven prodrug hydrogels for diabetic wound healing, ACS Appl. Mater. Interfaces 14 (47) (2022) 52643–52658.
[24] Y.L. Chen, C.C. Chang, Y.C. Lin, M.C. Chen, Double-layered PLGA/HA microneedle systems as a long-acting formulation of polyphenols for effective and long-term management of atopic dermatitis, Biomater. Sci. 11 (14) (2023) 4995–5011.
[25] J. Qin, S. Wei, H. Xu, L. Wang, P. Hao, B. Peng, Y. Zhang, P. Shi, X. Zan, The bioinspired facile method to efficiently generate diverse proteinosomes with pH switchable permeability, Adv. Mater. Interfac. 7 (14) (2020).
[26] S. Zhou, R. Yang, X. Xie, L. Wang, S. Zheng, N. Li, S. Tang, X. Zan, pH-responsive hexa-histidine metal assembly (HmA) with enhanced biocatalytic cascades as the vehicle for glucose-mediated long-acting insulin delivery, Adv. Sci. 10 (23) (2023) e2301771.
[27] H. Zhao, J. Huang, Y. Li, X. Lv, H. Zhou, H. Wang, Y. Xu, C. Wang, J. Wang, Z. Liu, ROS-scavenging hydrogel to promote healing of bacteria infected diabetic wounds, Biomaterials 258 (2020) 120286.
[28] M. Pertea, D. Kim, G.M. Pertea, J.T. Leek, S.L. Salzberg, Transcript-level expression analysis of RNA-seq experiments with HISAT, StringTie and Ballgown, Nat. Protoc. 11 (9) (2016) 1650–1667.
[29] M.I. Love, W. Huber, S. Anders, Moderated estimation of fold change and dispersion for RNA-seq data with DESeq2, Genome Biol. 15 (12) (2014) 550.
[30] B.T. Sherman, M. Hao, J. Qiu, X. Jiao, M.W. Baseler, H.C. Lane, T. Imamichi, W. Chang, DAVID: a web server for functional enrichment analysis and functional annotation of gene lists (2021 update), Nucleic Acids Res. 50 (W1) (2022) W216–w221.
[31] A. Subramanian, P. Tamayo, V.K. Mootha, S. Mukherjee, B.L. Ebert, M.A. Gillette, A. Paulovich, S.L. Pomeroy, T.R. Golub, E.S. Lander, J.P. Mesirov, Gene set enrichment analysis: a knowledge-based approach for interpreting genome-wide expression profiles, Proc. Natl. Acad. Sci. U. S. A. 102 (43) (2005) 15545–15550.
[32] D. Szklarczyk, R. Kirsch, M. Koutrouli, K. Nastou, F. Mehryary, R. Hachilif, A. L. Gable, T. Fang, N.T. Doncheva, S. Pyysalo, P. Bork, L.J. Jensen, C. von Mering, The STRING database in 2023: protein-protein association networks and functional enrichment analyses for any sequenced genome of interest, Nucleic Acids Res. 51 (D1) (2023) D638–d646.
[33] P. Shannon, A. Markiel, O. Ozier, N.S. Baliga, J.T. Wang, D. Ramage, N. Amin, B. Schwikowski, T. Ideker, Cytoscape: a software environment for integrated models of biomolecular interaction networks, Genome Res. 13 (11) (2003) 2498–2504.

[34] G.D. Bader, C.W. Hogue, An automated method for finding molecular complexes in large protein interaction networks, BMC Bioinf. 4 (2003) 2.
[35] M.M.C.B.J. Blaiszik, D.A. McIlroy, J.S. Moore, S.R. White, N.R. Sottos, Microcapsules filled with reactive solutions for self-healing materials, Polymer 50 (4) (2009) 990–997.
[36] L.Y. Foo, Proanthocyanidins: gross chemical structures by infrared spectra, Phytochemistry 20 (6) (1981) 1397–1402.
[37] L. Biao, S. Tan, Q. Meng, J. Gao, X. Zhang, Z. Liu, Y. Fu, Green synthesis, characterization and application of proanthocyanidins-functionalized gold nanoparticles, Nanomaterials 8 (1) (2018).
[38] I.F. Benzie, J.J. Strain, The ferric reducing ability of plasma (FRAP) as a measure of "antioxidant power": the FRAP assay, Anal. Biochem. 239 (1) (1996) 70–76.
[39] P. Ionita, The chemistry of DPPH(·) free radical and congeners, Int. J. Mol. Sci. 22 (4) (2021).
[40] D. Banerjee, U.K. Madhusoodanan, M. Sharanabasappa, S. Ghosh, J. Jacob, Measurement of plasma hydroperoxide concentration by FOX-1 assay in conjunction with triphenylphosphine, Clinica chimica acta; international journal of clinical chemistry 337 (1–2) (2003) 147–152.
[41] K.K. Mahapatra, S.R. Mishra, B.P. Behera, S. Patil, D.A. Gewirtz, S.K. Bhutia, The lysosome as an imperative regulator of autophagy and cell death, Cell. Mol. Life Sci. : CM 78 (23) (2021) 7435–7449.
[42] E.J. Blott, G.M. Griffiths, Secretory lysosomes, Nat. Rev. Mol. Cell Biol. 3 (2) (2002) 122–131.
[43] E. Ratto, S.R. Chowdhury, N.S. Siefert, M. Schneider, M. Wittmann, D. Helm, W. Palm, Direct control of lysosomal catabolic activity by mTORC1 through regulation of V-ATPase assembly, Nat. Commun. 13 (1) (2022) 4848.
[44] M. Abu-Remaileh, G.A. Wyant, C. Kim, N.N. Laqtom, M. Abbasi, S.H. Chan, E. Freinkman, D.M. Sabatini, Lysosomal metabolomics reveals V-ATPase- and mTOR-dependent regulation of amino acid efflux from lysosomes, Science (New York, N.Y.) 358 (6364) (2017) 807–813.
[45] M. Hu, J. Chen, S. Liu, H. Xu, The acid gate in the lysosome, Autophagy 19 (4) (2023) 1368–1370.
[46] P. Shi, J. Qin, S. Luo, P. Hao, N. Li, X. Zan, Effect of the stiffness of one-layer protein-based microcapsules on dendritic cell uptake and endocytic mechanism, Biomater. Sci. 10 (1) (2021) 178–188.
[47] M. Lei, C. Guo, L. Hua, S. Xue, D. Yu, C. Zhang, D. Wang, Crocin attenuates joint pain and muscle dysfunction in osteoarthritis rat, Inflammation 40 (6) (2017) 2086–2093.
[48] D.S. Chen, J.G. Cao, B. Zhu, Z.L. Wang, T.F. Wang, J.J. Tang, Baicalin attenuates joint pain and muscle dysfunction by inhibiting muscular oxidative stress in an experimental osteoarthritis rat model, Arch. Immunol. Ther. Exp. 66 (6) (2018) 453–461.
[49] M.K. Yadav, J. Maharana, R. Yadav, S. Saha, P. Sarma, C. Soni, V. Singh, S. Saha, M. Ganguly, X.X. Li, S. Mohapatra, S. Mishra, H.A. Khant, M. Chami, T. M. Woodruff, R. Banerjee, A.K. Shukla, C. Gati, Molecular basis of anaphylatoxin binding, activation, and signaling bias at complement receptors, Cell 186 (22) (2023) 4956–4973.e21.
[50] A. Menny, M. Serna, C.M. Boyd, S. Gardner, A.P. Joseph, B.P. Morgan, M. Topf, N. J. Brooks, D. Bubeck, CryoEM reveals how the complement membrane attack complex ruptures lipid bilayers, Nat. Commun. 9 (1) (2018) 5316.
[51] E.S. Parsons, G.J. Stanley, A.L.B. Pyne, A.W. Hodel, A.P. Nievergelt, A. Menny, A. R. Yon, A. Rowley, R.P. Richter, G.E. Fantner, D. Bubeck, B.W. Hoogenboom, Single-molecule kinetics of pore assembly by the membrane attack complex, Nat. Commun. 10 (1) (2019) 2066.
[52] F. Agostini, M. Bisaglia, N. Plotegher, Linking ROS levels to autophagy: the key role of AMPK, Antioxidants 12 (7) (2023).
[53] Z. Gong, K. Wang, J. Chen, J. Zhu, Z. Feng, C. Song, Z. Zhang, H. Wang, S. Fan, S. Shen, X. Fang, CircZSWIM6 mediates dysregulation of ECM and energy homeostasis in ageing chondrocytes through RPS14 post-translational modification, Clin. Transl. Med. 13 (1) (2023) e1158.
[54] B.B. Zhang, G. Zhou, C. Li, AMPK: an emerging drug target for diabetes and the metabolic syndrome, Cell Metabol. 9 (5) (2009) 407–416.
[55] T.P. Yang, H.M. Chen, C.C. Hu, L.Y. Chen, F.F. Shih, D.M. Tantoh, K.J. Lee, Y. C. Liaw, R.T. Tsai, Y.P. Liaw, Interaction of osteoarthritis and BMI on leptin promoter methylation in Taiwanese adults, Int. J. Mol. Sci. 21 (1) (2019).
[56] W. Liu, T. Jiang, W. Zheng, J. Zhang, A. Li, C. Lu, Z. Lin, FTO-mediated m6A demethylation of pri-miR-3591 alleviates osteoarthritis progression, Arthritis Res. Ther. 25 (1) (2023) 53.
[57] K. Hasegawa, Y. Sakamaki, M. Tamaki, S. Wakino, PCK1 protects against mitoribosomal defects in diabetic nephropathy in mouse models, J. Am. Soc. Nephrol. : JASN (J. Am. Soc. Nephrol.) 34 (8) (2023) 1343–1365.
[58] S. Wu, Q. Lu, Y. Ding, Y. Wu, Y. Qiu, P. Wang, X. Mao, K. Huang, Z. Xie, M.H. Zou, Hyperglycemia-driven inhibition of AMP-activated protein kinase α2 induces diabetic cardiomyopathy by promoting mitochondria-associated endoplasmic reticulum membranes in vivo, Circulation 139 (16) (2019) 1913–1936.
[59] S.P. Kalra, Pivotal role of leptin-hypothalamus signaling in the etiology of diabetes uncovered by gene therapy: a new therapeutic intervention? Gene Ther. 18 (4) (2011) 319–325.